ORIGINAL RESEARCH

Surface Modification of Wood Activated Carbon by CVD of NH₃ to Improve Its Micropore Volume and Adsorption to Carbamazepine

Xun Zhou [iD][1], Yue Zhong[2], Li He[3], Chengxin Sun [iD][2], Guoxue Xiao[1], Hong Luo[1], Rongfen Ran[1], Changying Wu[1], Ting Zhang[1], Shuiping Ou [iD][4], Yongke Zhong [iD][2]

[1]Department of Pharmacy, Dafang County People's Hospital, Bijie, Guizhou, 551600, People's Republic of China; [2]School of Pharmacy, Zunyi Medical University, Zunyi, Guizhou, 563000, People's Republic of China; [3]Department of Pharmacy, The First People's Hospital of Zunyi, Zunyi, Guizhou, 563000, People's Republic of China; [4]Department of Pharmacy, Affiliated Hospital of Zunyi Medical University, Zunyi, Guizhou, 563003, People's Republic of China

Correspondence: Shuiping Ou; Yongke Zhong, Email oushuiping1208@126.com; zhongyk2006@163.com

Objective: This study enhanced wood-activated carbon using ammonia chemical vapor deposition (NH₃-CVD) to improve its adsorption properties for carbamazepine (CBZ).

Methods: Modification was done in a vacuum tube sintering furnace. We used X-ray photoelectron spectroscopy (XPS), Brunauer–Emmett–Teller (BET) method, and Fourier Transform Infrared Spectroscopy (FTIR) for characterization and analysis. Kinetic adsorption and isothermal adsorption tests were carried out by UV spectrophotometry.

Results: NH₃-CVD significantly increased the micropore volume and surface area, notably in the *W-6* sample, and raised the nitrogen content on the carbon surface. The adsorption capacity of modified activated carbon (*W-7*) reached 130.81 mg/g, outperforming the unmodified (*W-0*) at 72.46 mg/g. FTIR results indicated strong hydrogen bonding with CBZ molecules.

Conclusion: NH₃-CVD modification improves CBZ adsorption on wood activated carbon by increasing micropore volume and enhancing hydrogen bonding, confirming a single-layer adsorption on a heterogeneous surface.

Keywords: nitrogen doped activated carbon, carbamazepine, chemical vapor deposition, hemoperfusion adsorbent

Introduction

Carbamazepine (CBZ), a classic antiepileptic drug approved in 1974, is widely acknowledged for its therapeutic efficacy. It exhibits a bioavailability of 58% to 85% and a high protein binding rate of approximately 80% to 85%.[1,2] Despite its effectiveness, CBZ poses challenges due to its complex metabolism, narrow therapeutic window, and significant individual differences in drug metabolism. Adverse drug reactions are not uncommon, as evidenced by Ding Yiduo et al's retrospective study, which highlighted CBZ's involvement in a substantial number of cases.[3] Blood perfusion is a blood purification method based on the principle of small molecule toxicants being adsorbed by adsorbents, typically activated charcoal. It is the most effective treatment method for Carbamazepine poisoning after it has been absorbed into the blood.[4–6] At present, there are many studies on the removal of carbamazepine by adsorption methods, and most of these studies are used for sewage treatment.[7,8] In contrast, this study is more inclined to discover a specific hemoperfusion adsorbent with stable physical and chemical properties.

In the wider context, pharmaceuticals and personal care products (PPCPs) have emerged as pollutants of concern, encompassing various antibiotics, painkillers, and antihypertensive drugs.[9] Among these, CBZ is often used as an indicator of PPCPs pollution due to its persistence in water bodies and high detectability.[10] This situation calls for an urgent need to develop efficient and practical methods for mitigating CBZ pollution in aquatic environments.[11,12]

Activated carbon, with its developed pore structure and excellent adsorption properties, is extensively utilized in environmental protection, medical treatment, scientific research, and other fields.[13] Notably, its application in medical

Graphical Abstract
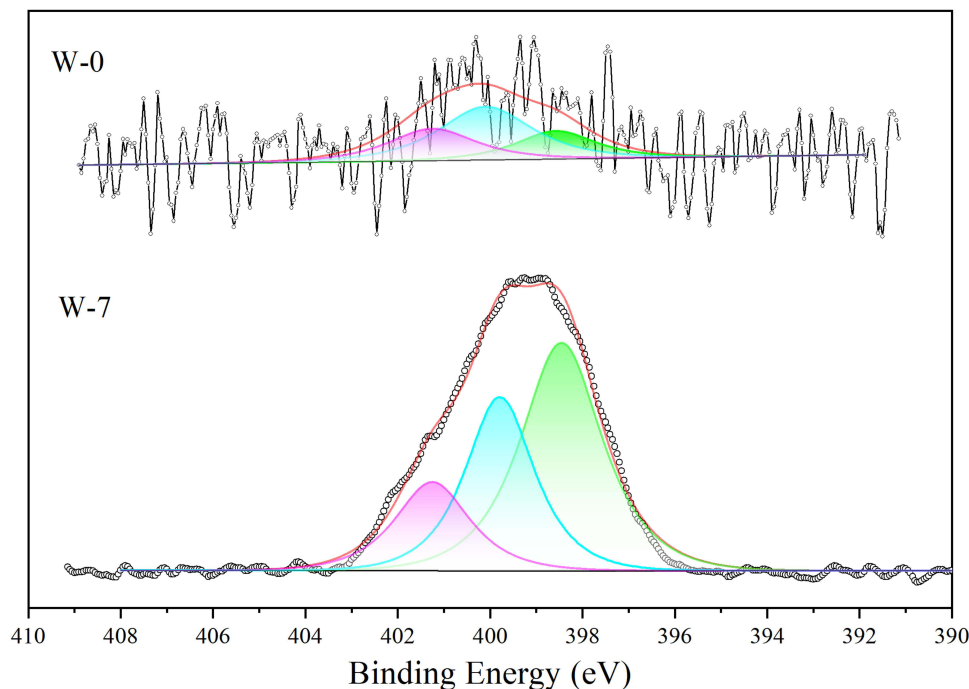
blood purification further highlights its versatility.[14,15] Within this framework, Chemical Vapor Deposition (CVD) emerges as a promising technique. CVD involves gaseous substances reacting on solids to produce solid sediments, encompassing steps like the formation of volatile substances, transportation of the reaction gas, and chemical reactions on solids to produce solid substances.[16] Our study explores the potential of CVD, specifically ammonia chemical vapor deposition (NH_3-CVD), in modifying activated carbon to enhance its efficacy in adsorbing CBZ from water bodies, addressing a critical environmental and public health issue.

Materials and Methods
Reagents and Instruments
Reagents
Carbamazepine (CBZ): > 99%, Shanghai Huzhen Biotechnology.

Ammonia Solution: (25–28%), Chongqing Chuandong Chemical Group.

Wood (Chinese fir) Activated Carbon: (80–100 mesh), Chengde Ji bei Yan Shan Activated Carbon.

Instruments
Thermal Stirrer: DF-*101S*, Gongyi Yuhua Instrument.

Sintering Furnace: *OTF Series*, Hefei Kejing Material Technology.

UV-Visible Spectrophotometer: *MODEL U-3010*, Hitachi.

Nitrogen Adsorption Instrument: *JW-BK122W*, Beijing Jing wei Gao bo.

XPS: *XSAM800*, Kratos.

FTIR: *Nicolet iS20*, Thermo Scientific.

Modification of Activated Carbon

In our experimental procedure, we modified wood activated carbon using ammonia chemical vapor deposition (NH_3-CVD). The process involved the following steps:

Preparation of Ammonia Gas

Measured 200.0 mL of ammonia water into a 500 mL round-bottom flask.

Conducted oil bath heating in three stages to release ammonia gas: first at 60°C for 30 minutes, then 80°C for 30 minutes, and finally at 100°C for 30 minutes.

Modification Process

Placed 10 g of wood activated carbon in a tubular furnace.

Initially, pumped N_2 (50 mL/min) to remove air from the furnace during the heating phase.

Once the temperature reached 700°C, introduced NH_3 (150 mL/min) into the furnace, maintaining this flow for 90 minutes.

Post-Reaction Treatment

After the reaction, allowed the activated carbon to cool to room temperature.

Washed the carbon with water until the pH stabilized, and then dried it for later use.

The modified activated carbon obtained at 700°C was labeled *W-7*.

Similarly, we modified additional samples of activated carbon at 600°C and 500°C, labeled as *W-6* and *W-5*, respectively. For comparison, wood activated carbon without NH_3 modification was washed to a constant pH and labeled as *W-0*.

Characterization of Activated Carbon

Pore Size Determination

Instrument

JW−BK122W Static Nitrogen Adsorption.

Methodology

Multi-point method.

Procedure

Degassed activated carbon at 120°C for 1 hour. Specific surface point range selected was between 0.05 and 0.3.

Adsorption Gas

Nitrogen.

Adsorption Temperature

Liquid nitrogen bath −196°C.

Surface Element Analysis (XPS)

Instrument

XSAM800 Multifunctional Surface Analysis Electron Spectrometer.

Settings

Al target X-ray gun operated at 12 kV × 15 mA. Background vacuum in analysis chamber maintained at 2×10^{-7} Pa.

Calibration

Spectrometer corrected with CU2P3/2, Ag3d5, and AU4F7/2 standard samples using FAT method; Data normalized to C1s peak at 284.8 eV.

3253

Scanning Parameters

Full spectrum scan step size: 150ms/0.65ev. Fine structure spectrum: 150 ms/0.05 ev.

Data Analysis

N1s nuclear grade spectral peaks fitted using XPSpeak software.

Infrared Detection (FTIR)

Instrument

Thermo Scientific Nicolet iS20 Infrared Spectrometer.

Settings

Detector: DTGS KBr; Beam splitter: KBr.; Sample scanning: 32 times.; Background scanning: 32 times.; Resolution: 4.000; Moving mirror speed: 0.4747.; Aperture: 80.00.

Kinetic Adsorption and Isothermal Adsorption

UV Spectrophotometry Analysis

Figure 1A: Shows CBZ scanning results in the λ (225–400) nm range. CBZ exhibited stable maximum absorption at $\lambda = 284\ nm$.

Figure 1B: Working curve for CBZ adsorption experiment with a correlation coefficient $R^2 = 0.9993$, indicating strong correlation between absorbance and concentration. The linear equation $y = 0.0477x + 0.0775$ was used for quantitative analysis.

Kinetic Adsorption Experiments

CBZ Solution

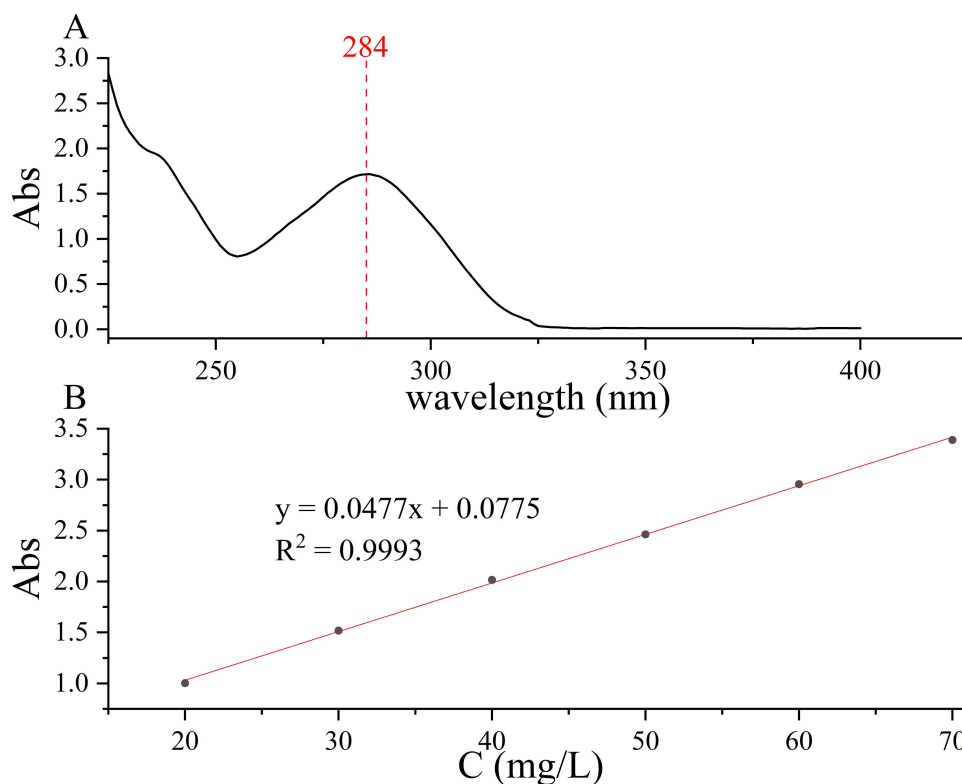Used 50 mg/L concentration for kinetic studies.

Figure 1 (**A**) UV scan of CBZ; (**B**) Working curve of adsorption experiments.

Contact Time Range
Experiments conducted over a period of 0 to 600 minutes.

Procedure
Weighed 0.030 g of activated carbon.
  Mixed it with 0.090 L of CBZ solution in a 150 mL conical flask.
  Placed the flask in a water bath shaker set at 37°C and 110 rpm.
  Measured absorbance of the supernatant at $\lambda = 284$ nm.

Calculation
Adsorption capacity (Q) determined using Lambert-Beer's law.

Lambert-Beer's Law Application
$$C_1/C_2 = A_1/A_2 \quad (1)$$
$$q_t = (C_0 - C_1)V/m \quad (2)$$

Equation
C_1 and C_2 are different concentrations of CBZ (mg/L) within the linear range; A_1 and A_2 are corresponding absorbance values. The adsorption capacity (q_t) at a specific time, C_e (the concentration at qt time), C_0 (initial concentration), V (volume of solution), and m (mass of activated carbon) were used in calculations.

Within a specific concentration range, there is a stable linear relationship between the concentration of carbamazepine solution and the absorbance. In the adsorption experiment, according to the linear equation, the concentration of the solution can be calculated by measuring the absorbance of the solution, and the adsorption capacity of the activated carbon for the drug can be calculated according to Formula (2).

Kinetic Models: Tested the fit of the data using intraparticle diffusion, Lagergren's quasi-first-order and quasi-second-order kinetic models to analyze adsorption kinetics.

Isothermal Adsorption Experiments
CBZ Solutions
Initial concentrations of 20, 30, 40, 50, 60, and 70 mg/L.

Contact Time Range
Experiments conducted over a period of 0 to 600 minutes.

Same Procedure
As kinetic experiments.

Isothermal Models
Performed fitting tests using Langmuir and Freundlich isothermal models to evaluate the adsorption process.

Results
Texture Results of Activated Carbon
In line with the International Union of Pure and Applied Chemistry (IUPAC) standards, pore sizes in powder materials are categorized as micropores (less than 2 nm), mesopores (2–50 nm), and macropores (greater than 50 nm). Our study's BET analysis revealed significant changes in the specific surface area and micropore volume of wood activated carbon following NH_3-CVD modification. Table 1 summarizes the main textural parameters of the activated carbon before and after modification.

The most notable observation was in sample *W-6*, which exhibited the largest increase in both specific surface area and micropore volume among the modified samples. The specific surface area and micropore volume of *W-6* were

Table 1 Texture of Modified Wood-Based Activated Carbon

Samples	S_{BET}(m²/g)	V_{total}(cm³/g)	V_{micro}(cm³/g)	Vmeso (cm³/g)	D_{BJH}(nm)
W-0	748.627	0.461	0.356	0.105	2.459
W-5	775.325	0.454	0.367	0.087	2.342
W-6	846.531	0.484	0.398	0.086	2.287
W-7	797.034	0.465	0.381	0.084	2.334

Abbreviations: S_{BET}, specific surface area; V_{total}, total pore volume; V_{micro}, micropore volume; Vmeso, mesoporous volume; D_{BJH}, average pore size.

measured at 846.531 m²/g and 0.398 cm³/g, respectively. This enhancement is crucial as micropore adsorption is reported to be the predominant mechanism for activated carbon to adsorb small molecular compounds.[9] Additionally, the micropore structure is a significant contributor to the overall specific surface area of activated carbon. Consequently, the observed increase in specific surface area and micropore volume is expected to significantly improve the adsorption performance of the activated carbon.

Figure 2 presents diagrams of micropores (A) and mesopores (B) in wood activated carbon before and after modification. The micropore size distribution is primarily within the range of 0.2 to 1.0 nm, while the mesopore size predominantly falls between 2.5 and 17 nm. Analyzing these diagrams in conjunction with the data in Table 1, we observe that the hierarchy in terms of micropore volume capacity is *W-6 > W-7 > W-5 > W-0*.
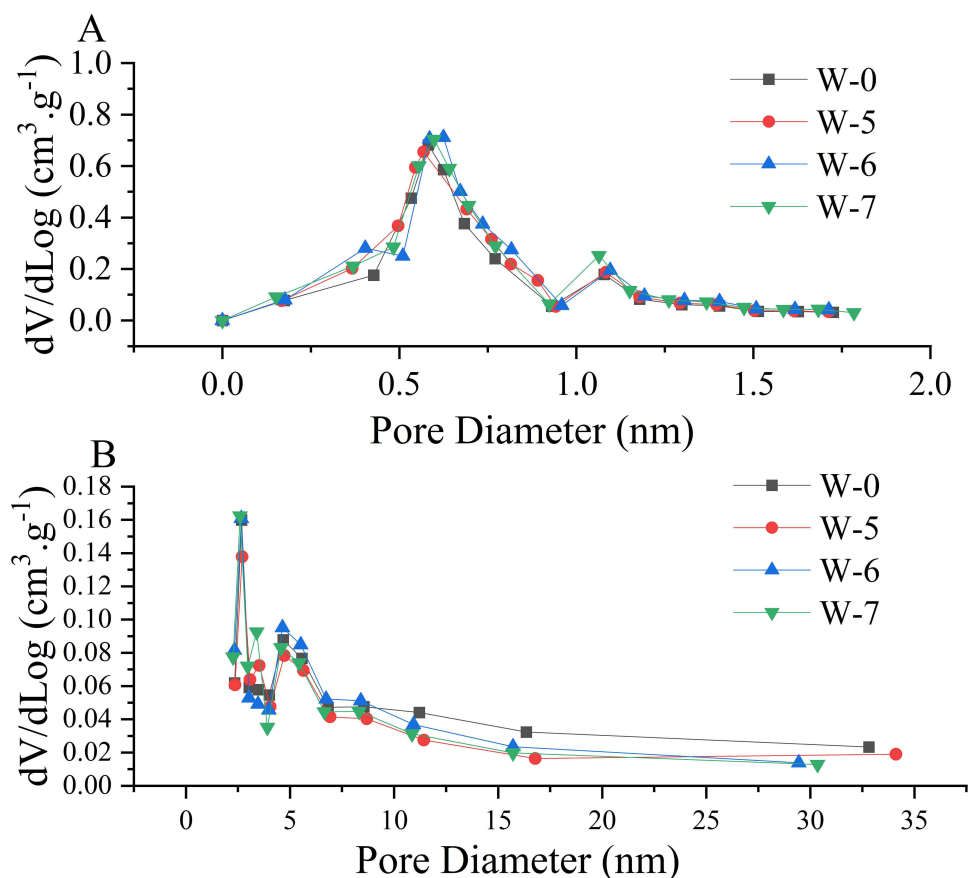

Figure 2 Pore volume and pore size distribution of wood activated carbon: (**A**) micropore, (**B**) mesopore.

Under our experimental conditions, an interesting phenomenon was noted: when the reaction temperature reaches 600°C, further temperature increase tends to disrupt the micro-pore structure of the activated carbon. The micropore volume of activated carbon first increases and then decreases with the increase of the modification reaction temperature. This effect was somewhat mitigated due to the original carbon's abundant micropore distribution, leading to a less pronounced increase in micropore volume post-modification, as evidenced in Figure 2A.

Furthermore, Figure 2B reveals a slight decrease in mesoporous volume following modification, aligning with the trends observed in Table 1. This suggests that the NH_3-CVD modification process, while enhancing micropore volume, may simultaneously lead to a reduction in mesoporous volume, impacting the overall porosity of the activated carbon.

X-Ray Photoelectron Spectroscopy (XPS) Analysis Results

Figure 3 depicts the XPS full spectrum analysis results, comparing wood activated carbon samples before and after the NH_3-CVD modification process. The analysis primarily identifies the presence of three elements: Carbon (C), Nitrogen (N), and Oxygen (O). Notably, the most significant change observed is in the nitrogen content on the surface of the activated carbon.

Prior to modification, the nitrogen content on the activated carbon's surface was markedly low. However, post-modification with NH_3-CVD, there is a substantial increase in the surface nitrogen content. This indicates that the modification process effectively incorporates nitrogen into the carbon structure, potentially altering its adsorption characteristics and chemical properties. The presence of almost no other elements except C, N, and O suggests the purity of the sample and the specificity of the modification effect.

Table 2 provides a detailed analysis of the main elements present on the surface of wood activated carbon, comparing the samples before and after NH_3-CVD modification. The data clearly demonstrates that the modification process substantially increases the nitrogen content on the surface of the activated carbon. Concurrently, there is a noticeable decrease in the percentage of oxygen elements following modification.

These alterations in elemental composition align with the results depicted in Figure 3. The increase in nitrogen content post-modification underscores the effectiveness of the NH_3-CVD process in altering the chemical properties of
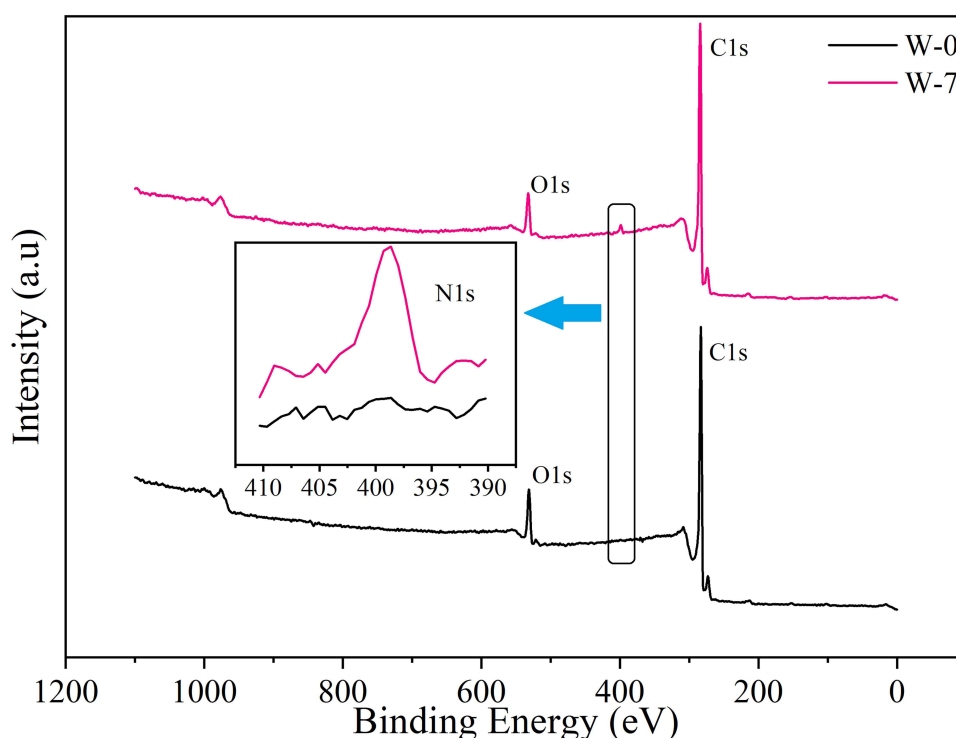

Figure 3 XPS Full spectrum of wood-based activated carbon before and after modification.

Table 2 Analysis of XPS Element Content in Wood Activated Carbon

Samples	C atom (%)	N atom (%)	O atom (%)
W-0	90.87	0.31	8.82
W-5	91.64	0.86	7.50
W-6	92.41	1.22	6.37
W-7	91.73	1.72	6.55

the activated carbon surface, potentially enhancing its adsorption capabilities. Simultaneously, the reduction in oxygen content further confirms the specificity of the modification effect, as the process primarily influences nitrogen integration while reducing oxygen presence. However, for adsorption, the action of oxygen is "supersaturated".

As shown in the Figure 4, Research indicates that nitrogen-doped activated carbon typically exhibits three primary forms of nitrogen:[17,18]

Pyridinic-N: In this form, nitrogen atoms replace carbon atoms in the six-membered rings of the activated carbon structure. This substitution alters the electronic and chemical properties of the carbon lattice.

Pyrrolic-N: This configuration involves the substitution of a carbon atom with a nitrogen atom in a five-membered ring. Pyrrolic nitrogen shares some characteristics with pyridinic nitrogen, influencing the carbon structure similarly.

Graphitic-N: Here, a nitrogen atom replaces a carbon atom in the activated carbon's lattice without creating a vacancy. It remains bonded to three carbon atoms, maintaining the integrity of the six-membered ring. This type of doping can impact the electronic properties of the carbon material.

These different nitrogen configurations contribute to the varied chemical and adsorption properties of nitrogen-doped activated carbon, influencing its effectiveness in specific applications.

Figure 5 illustrates the binding energy peaks identified in the XPS analysis of the modified wood activated carbon. These peaks correspond to the different nitrogen configurations within the carbon structure:
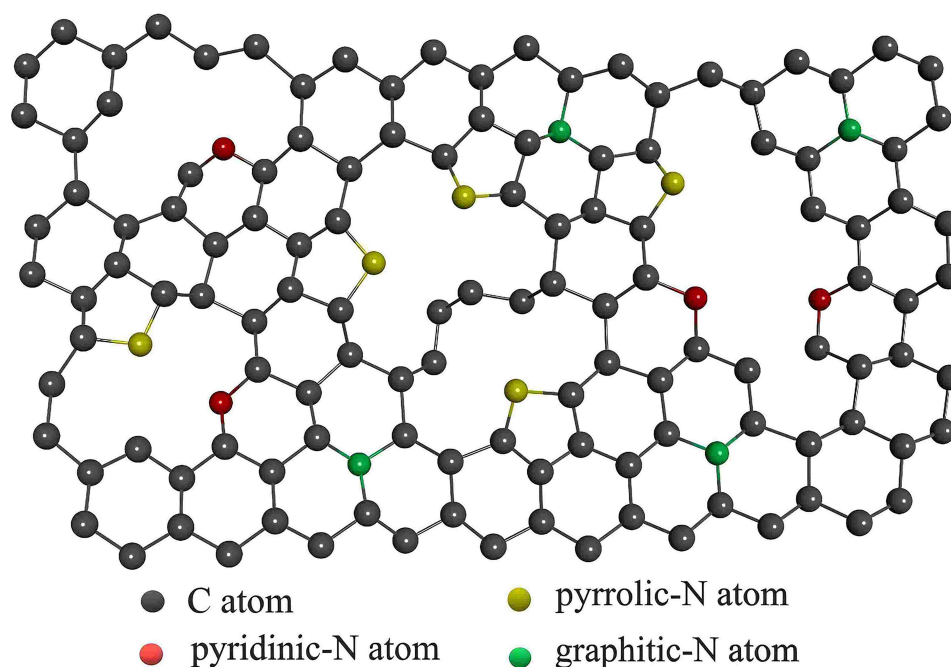
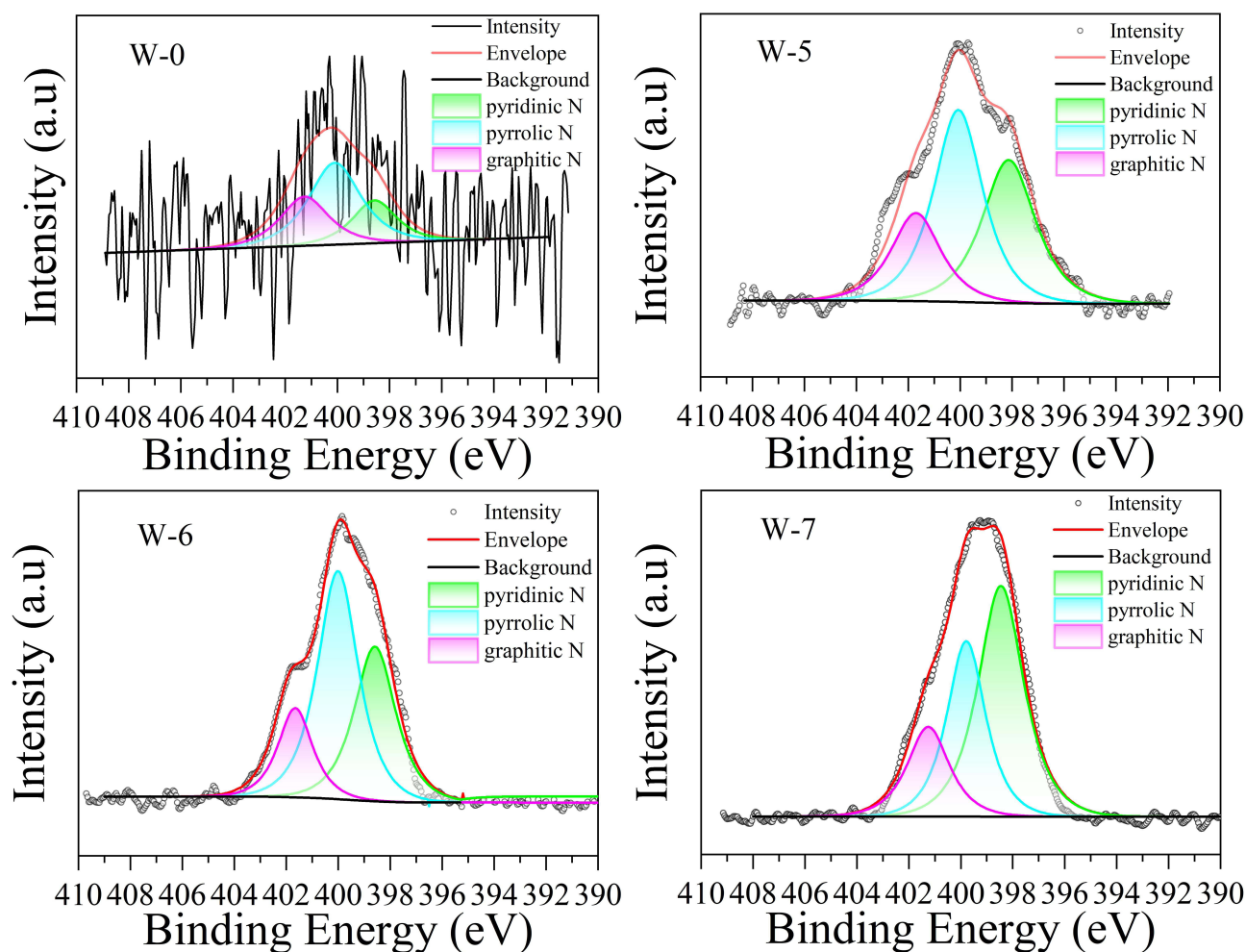**Figure 4** 3D diagram of Three main forms of N in activated carbon.

Figure 5 N1s XPS spectra for W-0, W-5, W-6 and W-7.

Pyridinic-N: A peak at 398.5 ± 0.3 eV indicates the presence of pyridinic-N, where nitrogen atoms are incorporated into six-membered rings, replacing carbon atoms.

Pyrrolic-N: The peak at 400.20±0.3 eV is attributed to pyrrolic-N, representing nitrogen atoms substituting for carbon atoms in five-membered rings.

Graphitic-N: A peak at 401.3±0.3 eV signifies graphitic-N, where nitrogen atoms replace carbon atoms in the lattice, retaining the structure of the six-membered rings.

These findings, consistent with literature,[19–21] confirm the successful doping of nitrogen in various structural forms within the activated carbon, potentially enhancing its adsorptive properties and chemical interactions.

Utilizing the Lorentz-Gaussian function, we fitted the fine structure spectrum of nitrogen in four activated carbon samples using XPSpeak software. The calculated contents of each nitrogen component are detailed in Table 3. When correlated with the findings from Figure 5, it becomes evident that NH_3-CVD modification not only increases the total nitrogen content on the surface of activated carbon but also alters the proportion of the three nitrogen chemical states.

Post-modification, the content of graphitic-type nitrogen decreased in the *W-5, W-6*, and *W-7* samples. Interestingly, as the modification temperature varied between 500°C and 700°C, the predominant form of nitrogen in the samples changed: at 600°C, pyrrolic nitrogen was the primary form, while at 700°C, pyridinic nitrogen dominated. This shift suggests that at higher temperatures, the carbon-NH_3 reaction intensifies, facilitating a rearrangement of *C-N* bonds towards a more stable chemical state, namely pyridinic nitrogen.[22,23]

**Table 3** XPS N1s Data Analysis of Wood-Based Activated Carbon

Samples	Pyridinic-N (%)	Pyrrolic-N (%)	Graphitic-N (%)
W-0	22.21	49.78	28.01
W-5	35.46	44.21	20.33
W-6	32.19	51.07	16.74
W-7	49.97	32.22	17.81

The study also delves into the role of hydrogen bonding as a major contributor to intermolecular forces. Hydrogen bonding occurs due to electron cloud skewing when hydrogen atoms covalently bond with highly electronegative atoms like fluorine, oxygen, or nitrogen. This leaves the hydrogen atom electron-deficient and the electronegative atom electron-rich, leading to an attraction between hydrogen atoms in one molecule and electronegative atoms in another.

In the context of activated carbon, graphitic nitrogen, bonded with three carbon atoms, exhibits a balanced electron cloud distribution with similar electron absorption abilities as carbon, thus unable to form hydrogen bonds with CBZ molecules. Conversely, pyridinic and pyrrolic nitrogen, bonded with two carbon atoms and one hydrogen atom, can easily form hydrogen bonds with CBZ molecules. This capability significantly enhances the adsorption performance of CBZ on activated carbon, as these forms of nitrogen provide active sites for hydrogen bonding.

Kinetic Adsorption Experiment

Figure 6 illustrates the time-dependent adsorption capacity of wood activated carbon for CBZ, both before and after NH_3-CVD modification. The graph clearly shows a significant change in the adsorption capacity of the samples post-modification. Compared to the unmodified carbon, the three activated carbons treated with NH_3-CVD exhibited superior adsorption and removal abilities for CBZ.
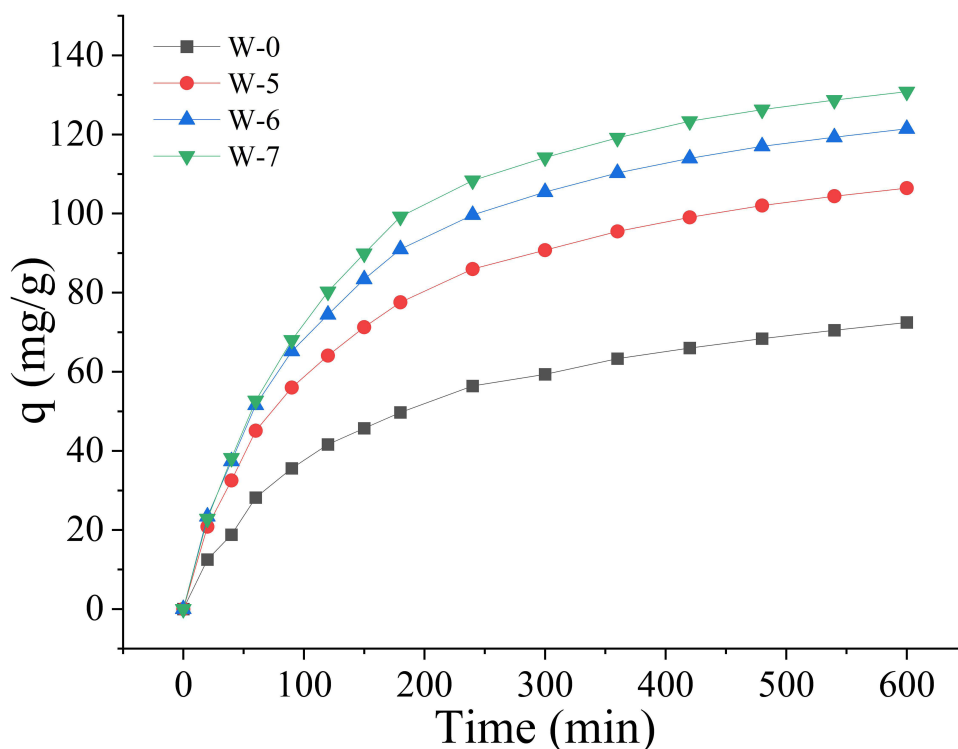
Figure 6 Dynamic adsorption curve of wood-based activated carbon.

A key observation from the figure is that the majority of CBZ adsorption occurs within the first 4 hours. Initially, the concentration of CBZ in the solution decreases rapidly as it is adsorbed onto the activated carbon. However, after 4 hours, the rate of adsorption slows down. This change is attributed to the transition from adsorption driven by concentration differences to a state nearing adsorption saturation, where the concentration of CBZ in the activated carbon increases, and the driving force for further adsorption diminishes.

Consequently, beyond the 4-hour mark, there is no significant increase in the adsorption amount with the extension of time, indicating that the activated carbon approaches its adsorption capacity limit. This finding is critical in understanding the adsorption dynamics of CBZ on activated carbon and optimizing the use of NH_3-CVD modified carbon for efficient CBZ removal.

To comprehensively examine the adsorption characteristics of CBZ on activated carbon samples, we applied Intraparticle diffusion, Lagergren's quasi-first-order and quasi-second-order kinetic equations for kinetic fitting of the adsorption process.[24–26] These models are instrumental in deciphering the adsorption kinetics and are defined by their respective dynamic equations:

Intraparticle diffusion model: $q_t = Kt^{1/2} + C$ (3)

Pseudo−first−order model: $In(q_e - q_t) = Inq_e - K_1 t$ (4)

Pseudo−second−order model: $t/q_t = 1/K_2 q_e^2 + t/q_e$ (5)

These models are defined by key parameters that describe the adsorption process:

t: Adsorption time (minutes); *K:* Intraparticle diffusion rate constant (mg/g•min$^{1/2}$); *C:* Adsorption constant (mg/g), reflecting the boundary layer effect, calculated based on the intercept of the fitted straight line. q_t: Represents the adsorption capacity (mg/g) of CBZ at any given time (mg/g). q_e: Denotes the maximum adsorption capacity (mg/g) when the adsorption process reaches equilibrium. *($R_{O, T, 1, 2}$)²:* is the correlation coefficient of the fitting. K_1 and K_2: These are the rate constants for the quasi-first-order and quasi-second-order kinetics, respectively.

The intraparticle diffusion fitting parameters are listed in Table 4. The C value is not equal to zero, indicating that both physical adsorption and chemical adsorption exist in the adsorption process. According to the characteristics of the two adsorption types, it can be known that stage one is physical adsorption and stage two is chemical adsorption. By comparing the K_O and K_T values, it can be known that physical adsorption is the main adsorption method for carbamazepine by the four activated carbon samples.

By fitting our experimental data to these models, we quantitatively analyzed the rate and extent of CBZ adsorption on both unmodified and NH_3-CVD modified activated carbon. Figure 7 in our study illustrates this fitting, showcasing diagrams of the kinetic adsorption of CBZ. These diagrams provide a comparative visual representation of the adsorption behavior before and after the modification, highlighting the differences in adsorption kinetics and capacities brought about by the NH_3-CVD process.

Table 5 outlines the parameters derived from the kinetic analysis of CBZ adsorption on activated carbon. These parameters were calculated from the slope and intercept obtained from the linear equations fitted using the quasi-first-order and quasi-second-order dynamic models. Notably, the saturated adsorption capacity values, as determined by the quasi-first-order kinetics, closely align with the actual measured values. This is further supported by the high correlation coefficients *(R_1)²*, all exceeding 0.987. Such strong linear correlation indicates that the quasi-first-order kinetic model fitting is robust and reliable.

Table 4 Fitting Parameters of Intraparticle Diffusion Mode

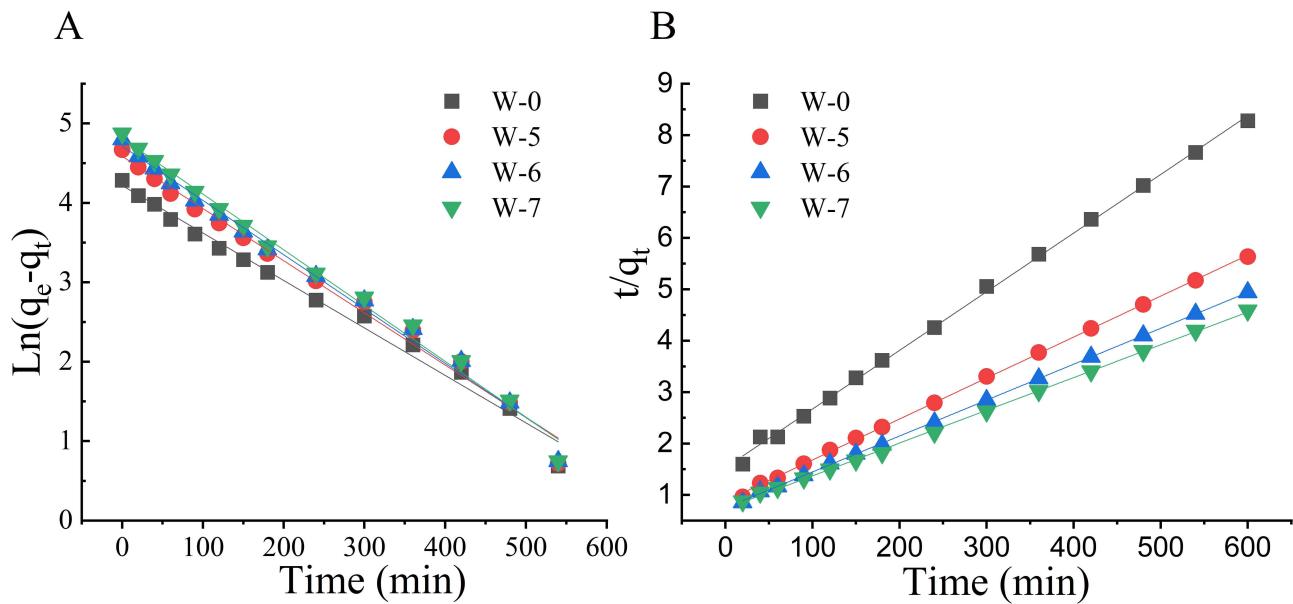| Adsorbent	Stage One			Stage Two		
	K_O	C_O	$(R_O)^2$	K_T	C_T	$(R_T)^2$
W-0	4.285	−6.424	0.997	1.811	28.473	0.991
W-5	6.387	−6.510	0.993	2.291	51.246	0.995
W-6	7.609	−9.370	0.998	2.407	63.625	0.986
W-7	8.612	−15.109	0.995	2.497	70.908	0.986

Figure 7 (**A**) Dynamics fitting of quasi-first-order; (**B**) Dynamics fitting of quasi-second-order.

Furthermore, the consistency of these results with the theoretical expectations of the model suggests that the adsorption behavior in our system is predominantly characterized by single-layer adsorption.[27] This finding is crucial for understanding the mechanism of CBZ adsorption on activated carbon, particularly in highlighting the efficiency and nature of the adsorption process post-NH_3-CVD modification.

Isothermal Adsorption Experiment

In our investigation, we explored how the adsorption capacity of activated carbon samples varied in CBZ solutions with different initial concentrations, keeping the volume of the CBZ solution and the mass of the activated carbon sample constant.

As demonstrated in Figure 8, a notable trend was observed. When the initial CBZ concentration was below 50 mg/L, the adsorption capacity (qe value) of the activated carbon increased significantly with the rising concentration of CBZ. However, beyond this concentration threshold (above 50 mg/L), the increase in adsorption capacity plateaued, showing no substantial rise with further increases in CBZ concentration.

This phenomenon can be explained by the limited number of available adsorption sites on the activated carbon. At lower drug concentrations, the number of CBZ molecules per unit volume of the solution is the primary factor influencing the adsorption capacity. Yet, as the concentration reaches and exceeds 50 mg/L, each adsorption site becomes surrounded by sufficient CBZ molecules for adsorption. Consequently, beyond this concentration, the number of adsorption sites becomes the limiting factor,

Table 5 Fitting Parameters of the Dynamic Mode

Adsorbent	q_e (mg/g)	First Order Kinetic Fitting Curve			Second Order Kinetic Fitting Curve		
		q_f(mg/g)	10^2*k_1	$(R_1)^2$	q_s(mg/g)	10^4*k_2	$(R_2)^2$
W-0	72.462	67.917	0.598	0.987	87.642	1.245	0.998
W-5	106.423	98.100	0.657	0.988	125.471	1.001	0.999
W-6	121.413	111.549	0.683	0.991	143.062	0.906	0.999
W-7	130.805	123.110	0.702	0.992	156.986	0.797	0.999

Notes: q_e is the actual maximum adsorption capacity, q_f and q_s are the maximum theoretical adsorption capacity obtained by first-order and second-order kinetics fitting, respectively.
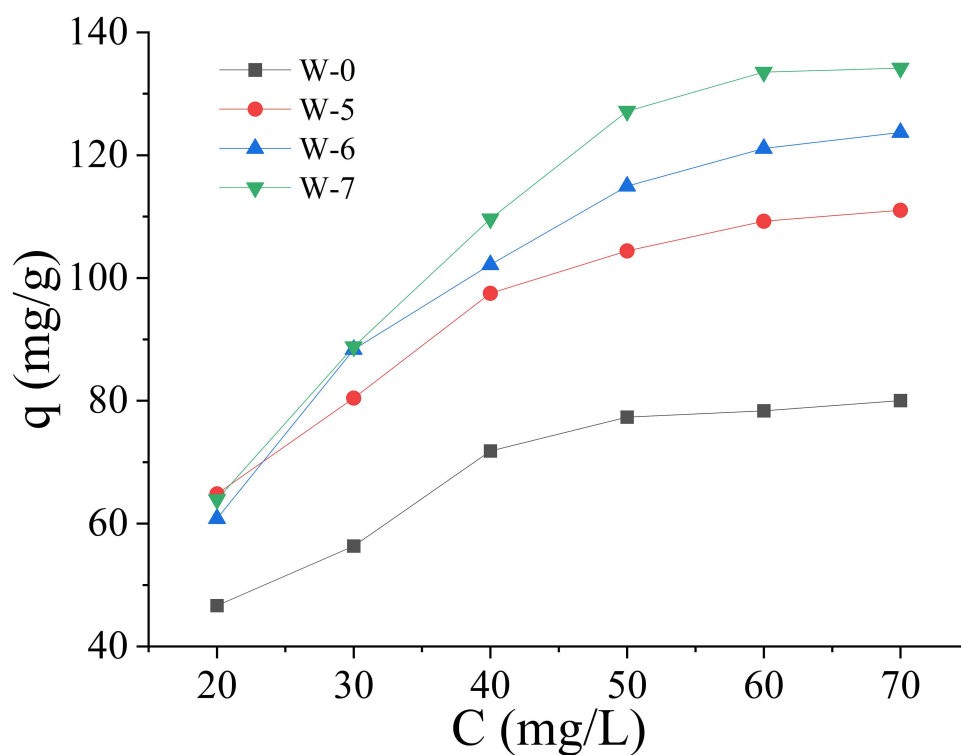
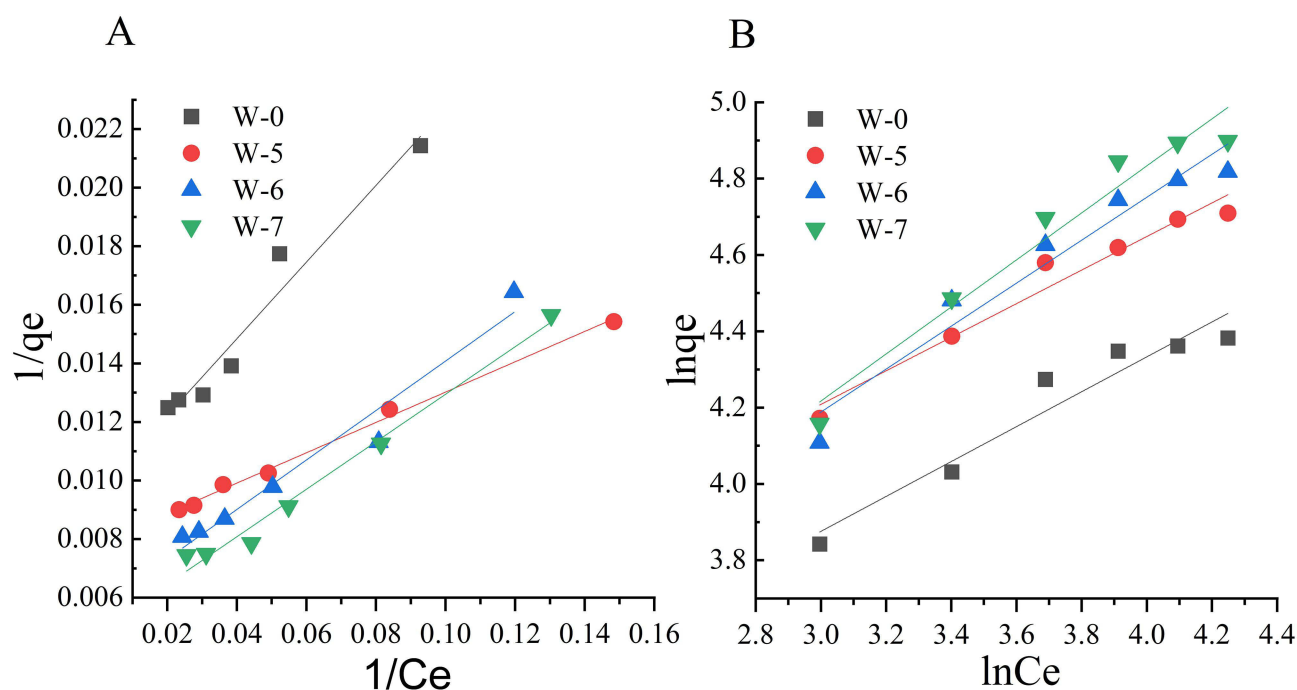**Figure 8** Isothermal adsorption curve of wood-based activated carbon.

Figure 9 Fitting diagram of Langmuir (**A**) and Freundlich (**B**) models.

not the concentration of the drug in the solution.[28] Hence, even with continued increases in CBZ concentration, the adsorption capacity of the activated carbon does not show significant enhancement.

To further clarify the adsorption mechanism of CBZ on wood activated carbon, Langmuir and Freundlich mathematical models were used to fit the adsorption behavior. Langmuir model: assume that the adsorption process occurs on a uniform surface.[27–29] and its linear form is as follows:

Langmuir model: $1/q_e=1/q_m+1/(q_mC_eK_L)$ (6)

The adsorption fitting figure is shown in Figure 9A, where $\boldsymbol{K_L}$ is the fitting constant of Langmuir model, $\boldsymbol{C_e}$ is the equilibrium concentration (mg/L), $\boldsymbol{q_e}$ is the adsorption amount at equilibrium (mg/g), and $\boldsymbol{q_m}$ is the theoretical maximum adsorption amount (mg/g). $\boldsymbol{(R_L)^2}$ is the correlation coefficient of the fitting.

Freundlich model: Assuming that the adsorption behavior occurs on the non-uniform surface, the adsorption situation depends on the distribution of active sites and exponential energy on the carbon surface, and its linear form is as follows:[24]

Freundlich model: $Inq_e=InK_F+(InC_e)1/n$ (7)

Where $\boldsymbol{k_F}$ is Freundlich constant (heterogeneous factor), $\boldsymbol{n}$ value is related to adsorption affinity. $\boldsymbol{(R_F)^2}$ is the correlation coefficient of the fitting. When $1 < n < 10$ indicates that the adsorption effect is good, indicating that the adsorption equilibrium tends to the occurrence of adsorption behavior.[30] In Figure 9B, the parameters k_F and n can be calculated by the intercept and slope of the fitting curve.

In Table 6, the Langmuir model fitting correlation coefficient $(R_L)^2$ ranges from 0.947 to 0.995, while the Freundlich model yields correlation coefficients $(R_F)^2$ between 0.917 and 0.952. Therefore, the Langmuir model exhibits a superior goodness of fit. However, it is noteworthy that there exists a substantial deviation between the maximum adsorption capacity q_m obtained from Langmuir fitting and the actual value q_e. Considering relevant reports,[31] we conclude that the Freundlich model aligns better with the isothermal curve study.

In the Freundlich fitting results, n values greater than 1 and less than 10 indicate that the adsorption of CBZ by wood activated carbon is a favorable removal process occurring on heterogeneous surfaces.

Experimental Results of Infrared Detection

Figure 10 displays the infrared spectrum scanning results of *W-0, W-7*, and *W-7X* samples, with sample *W-7X* obtained through saturated adsorption of CBZ on sample *W-7*. Analyzing the results in conjunction with the XPS analysis, the wide peak signal in the wavenumber range of 3700 to 3000 is attributed to *N-H* and *O-H* stretching vibration. Notably, in the figure, the signal at 3430 for *W-7X* is significantly stronger than that of the other two samples and is even comparable to the signal at wavenumber 1000 for *W-7X*.

As mentioned before, the doping of nitrogen elements on the surface of activated carbon is beneficial for the formation of intermolecular hydrogen bonds with carbamazepine molecules. Based on relevant reports, the peak range of infrared spectra for intermolecular hydrogen bonding falls within the interval (3550–3400), the presence of hydrogen bonds significantly enhances the infrared absorption in this region.[32,33] This observation implies that there are numerous intermolecular hydrogen bonds in the *W-7X* samples. These results provide further evidence that the formation of intermolecular hydrogen bonds is a crucial factor contributing to the effective adsorption of CBZ on wood activated carbon.

Table 6 Fitting Parameters of Langmuir and Freundlich Models

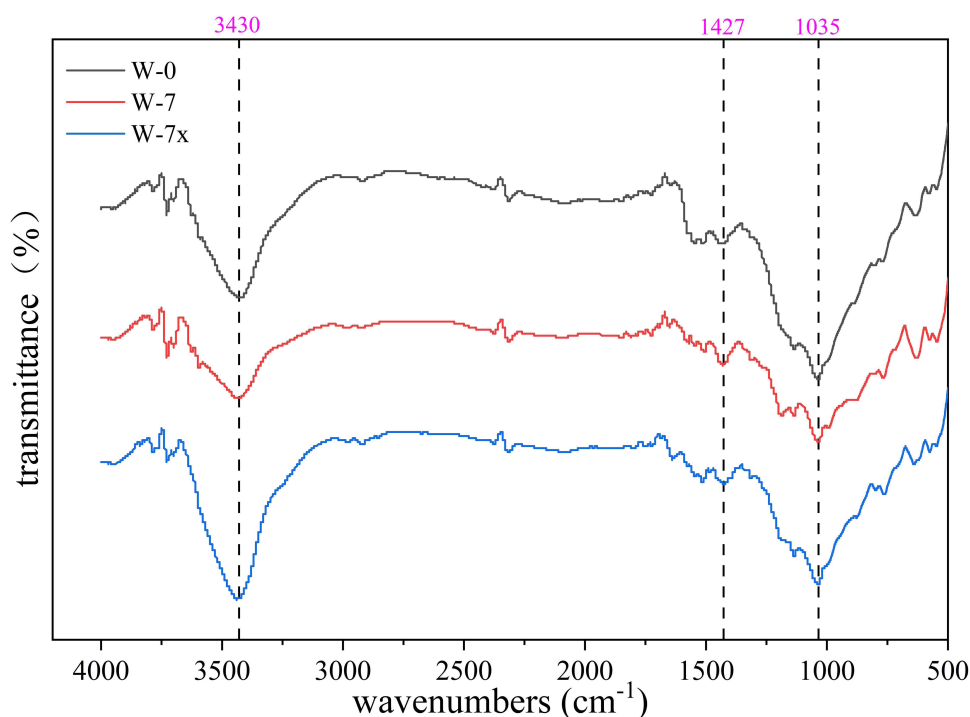| Adsorbent	q_e (mg/g)	Langmuir Fitting			Freundlich Fitting		
		q_m(mg/g)	K_L	$(R_L)^2$	K_F	n	$(R_F)^2$
W-0	80.050	104.058	0.073	0.947	12.232	2.187	0.917
W-5	111.026	127.551	0.151	0.995	17.968	2.273	0.952
W-6	123.714	177.305	0.067	0.951	12.179	1.776	0.930
W-7	134.164	206.612	0.059	0.982	10.684	1.623	0.945

Figure 10 Infrared detection results (W-7x: Sample W-7 saturated adsorption of CBZ).

Conclusion and Discussion

This study demonstrates that NH$_3$-CVD modification significantly enhances the adsorption performance of wood activated carbon for carbamazepine (CBZ). The modification increases the micropore volume, crucial for small molecule drug adsorption. Furthermore, the increased nitrogen content on the activated carbon surface, particularly in the form of pyridine and pyrrole nitrogen, facilitates hydrogen bonding with CBZ, enhancing adsorption. This explains why *W-7*, despite having a smaller surface area and micropore volume than *W-6*, shows greater CBZ adsorption capacity. Kinetic adsorption experiments align well with the quasi-first-order kinetic model; among the isothermal adsorption models, the Freundlich model accurately reflects CBZ adsorption on wood activated carbon, suggesting that CBZ adsorption on wood activated carbon is a single-layer process on heterogeneous surfaces.

The introduction of nitrogen into activated carbon has been a focus in recent research, It does not damage the structural stability of activated carbon but enhancing adsorption properties. The present study has demonstrated that NH$_3$-CVD modified wood activated carbon can significantly enhance the adsorption capacity of activated carbon for CBZ; and the potential applications of this new type of adsorbent material in the fields of environmental protection and medical have been effectively explored before the improvement of blood compatibility studies.

Funding

Disclosure

The authors report no conflicts of interest in this work.

References

1. Yang X, Xin S, Zhang Y, et al. Early hemoperfusion for emergency treatment of carbamazepine poisoning. *Am J Emergency Med*. 2018;36 (6):926–930. doi:10.1016/j.ajem.2017.10.048

2. Milovanovic DD, Milovanovic JR, Radovanovic M, et al. The influence of on carbamazepine serum concentration in epileptic pediatric patients. *Balkan J Med Genet*. 2016;19(1):21–28. doi:10.1515/bjmg-2016-0003

3. Ding Y, Qian Y, Gao J, et al. Clinical analysis of 84 cases of adverse drug reactions induced by antiepileptic drugs. *Pharm Care Res*. 2017;17 (06):457–460.

4. Lin T, Wei C, Sun S, et al. Analysis and monitoring of clinical pharmacists' rescue medication for children with carbamazepine poisoning. *Eval Anal Drug-Use Hosp China*. 2018;18(09):1264–1266.

5. Yu Q, Jianhui Z, Zhao X, et al. Clinical development of adsorption materials in blood purification. *Chin J Kidney Dis Invest*. 2021;10(03):170–174.

6. Guo J. Efficacy observation of children with carbamazepine poisoning treated with lipid emulsion. *Sichuan Med J*. 2018;39(08):913–916.

7. Yang J, Yang Z, Li J, et al. Engineering a hollow bowl-like porous carbon-confined Ru-MgO hetero-structured nanopair as a high-performance catalyst for ammonia borane hydrolysis. *Mater Horizons*. 2024;11(8):2032–2040. doi:10.1039/D3MH01909H

8. Zayyat RM, Yahfoufi R, Al-Hindi M, et al. Elucidating the dynamics of carbamazepine uptake using date pit-derived activated carbon: a comprehensive kinetic and thermodynamic analysis. *Heliyon*. 2024;10(20):e39068. doi:10.1016/j.heliyon.2024.e39068

9. Wang S, Hu Y, Wang J. Strategy of combining radiation with ferrate oxidation for enhancing the degradation and mineralization of carbamazepine. *Sci Total Environ*. 2019;687:1028–1033. doi:10.1016/j.scitotenv.2019.06.189

10. He Z, Xing Y, Zhang J, et al. Synthesis and degradation of carbamazepine by Mg-ZnO photocatalyst. *Technol Water Treat*. 2022;48(12):24–28.

11. JianJun L, Qin H, HuaiLi Z, et al. Molecular simulation and adsorption mechanism of carbamazepine imprinted adsorbent. *Chin J Anal Chem*. 2019;47(06):846–854.

12. Atugoda T, Vithanage M, Wijesekara H, et al. Interactions between microplastics, pharmaceuticals and personal care products: implications for vector transport. *Environ Int*. 2021;149:106367. doi:10.1016/j.envint.2020.106367

13. Wang B. Study on the preparation of microporous activated carbon and its adsorption property for CH_4/N_2. *Leather Chemicals*. 2021;38(01):16–19.

14. Gerashchenko BI, Nikolaev VG. Tackling the acute radiation syndrome: hemoperfusion with activated carbon revisited. *Med Hypotheses*. 2021;146:110430. doi:10.1016/j.mehy.2020.110430

15. Li Q, Zhang L. Progress of hemoadsorbent materials for hemoperfusion. *CIESC J*. 2020;71(S2):12–23.

16. Leigh WGS, Thomas ELH, Cuenca JA, et al. In-situ monitoring of microwave plasma-enhanced chemical vapour deposition diamond growth on silicon using spectroscopic ellipsometry. *Carbon*. 2023;202:204–212. doi:10.1016/j.carbon.2022.10.049

17. Hao G, Li W-C, Qian D, et al. Rapid synthesis of nitrogen-doped porous carbon monolith for CO_2 capture. *Adv Mater*. 2010;22(7):853–857. doi:10.1002/adma.200903765

18. Kang W, Quan H, Huang Y, et al. Recent advances in the synthesis and applications of nitrogen-doped graphene. *Hans J Nanotechnol*. 2019;9 (1):17–31. doi:10.12677/NAT.2019.91003

19. Li D, Zhou J, Zhang Z, et al. Improving low-pressure CO_2 capture performance of N-doped active carbons by adjusting flow rate of protective gas during alkali activation. *Carbon*. 2017;114:496–503. doi:10.1016/j.carbon.2016.12.039

20. Kou J, Sun L. Nitrogen-doped porous carbons derived from carbonization of a nitrogen-containing polymer: efficient adsorbents for selective CO_2 capture. *Ind Eng Chem Res*. 2016;55(41):10916–10925. doi:10.1021/acs.iecr.6b02857

21. Tian W, Zhang H, Sun H, et al. Heteroatom (N or N-S)-doping induced layered and honeycomb microstructures of porous carbons for CO_2 capture and energy applications. *Adv Funct Mater*. 2016;26(47):8651–8661. doi:10.1002/adfm.201603937

22. Liu H, Zhang J, Zheng C, et al. Quantum chemical study of the pyrolysis stability of pyrrolic nitrogen and pyridinic nitrogen in coal. *J Huazhong Univ Sci Technol*. 2004;11:13–15.

23. To J-W-F, He J, Mei J, et al. Hierarchical N-doped carbon as CO_2 adsorbent with high CO_2 selectivity from rationally designed polypyrrole precursor. *J Am Chem Soc*. 2016;138(3):1001–1009. doi:10.1021/jacs.5b11955

24. Sivamani S, N PBS, Nithya K, et al. Back-propagation neural network: box–Behnken design modelling for optimization of copper adsorption on Orange zest biochar. *Int J Environ Sci Technol*. 2022;19(5):4321–4336. doi:10.1007/s13762-021-03411-1

25. Liu C, Zhang M, Gao H, et al. Cyclic coupling of photocatalysis and adsorption for completely safe removal of N-nitrosamines in water. *Water Res*. 2022;209:117904. doi:10.1016/j.watres.2021.117904

26. Wang J, Guo X. Rethinking of the intraparticle diffusion adsorption kinetics model: interpretation, solving methods and applications. *Chemosphere*. 2022;309:136732. doi:10.1016/j.chemosphere.2022.136732

27. Mohamed HG, Aboud AA, Abd El-Salam HM. Synthesis and characterization of chitosan/polyacrylamide hydrogel grafted poly (N-methylaniline) for methyl red removal. *Int J Biol Macromol*. 2021;187:240–250. doi:10.1016/j.ijbiomac.2021.07.124

28. Ait Haki M, Imgharn A, Aarab N, et al. Efficient removal of crystal violet dye from aqueous solutions using sodium hydroxide-modified avocado shells: kinetics and isotherms modeling. *Wat Sci Technol*. 2022;85(1):433–448. doi:10.2166/wst.2021.451

29. Guo X, Wang J. Comparison of linearization methods for modeling the Langmuir adsorption isotherm. *J Mol Liq*. 2019;296:111850. doi:10.1016/j.molliq.2019.111850

30. Saravanan A, Kumar PS, Renita AA. Hybrid synthesis of novel material through acid modification followed ultrasonication to improve adsorption capacity for zinc removal. *J Cleaner Prod*. 2018;172:92–105. doi:10.1016/j.jclepro.2017.10.109

31. Bayram O, Köksal E, Göde F, et al. Decolorization of water through removal of methylene blue and malachite green on biodegradable magnetic Bauhinia variagata fruits. *Int J Phytorem*. 2022;24(3):311–323. doi:10.1080/15226514.2021.1937931

32. Dong X, Guo L, Dong X, et al. Quantitative analysis of microstructure of different coals by Fourier transform infrared spectroscopy. *China Sciencepaper*. 2022;17(01):55–61.

33. Yuan X, Zheng D, Wang X, et al. Unconventional O-H···C hydrogen bonding and effects of conformational changes on infrared spectroscopy of o-Cresol o -Cresol in solutions. *J Phys Chem*. 2016;120(51):10196–10206. doi:10.1021/acs.jpca.6b06945